JOURNAL OF ENVIRONMENTAL SCIENCES 101 (2021) 205–216

Available online at www.sciencedirect.com

ScienceDirect

www.elsevier.com/locate/jes

JES JOURNAL OF ENVIRONMENTAL SCIENCES

www.jesc.ac.cn

Interactions of extracellular DNA with aromatized biochar and protection against degradation by DNase I

Jing Fang[1,3], *Liang Jin*[2,3], *Qingkang Meng*[2,3], *Dengjun Wang*[4], *Daohui Lin*[2,*]

[1] *Key Laboratory of Recycling and Eco-treatment of Waste Biomass of Zhejiang Province, Zhejiang University of Science and Technology, Hangzhou 310023, China*

[2] *Department of Environmental Science, Zhejiang University, Hangzhou 310058, China*

[3] *School of Environmental Science and Engineering, Zhejiang Gongshang University, Hangzhou 310012, China*

[4] *Oak Ridge Institute for Science and Education (ORISE) Resident Research Associate, United States Environmental Protection Agency, Ada, OK 74820, USA*

ARTICLE INFO

Article history:
Received 4 June 2020
Revised 18 August 2020
Accepted 18 August 2020
Available online 2 September 2020

Keywords:
Aromatized biochar
Extracellular DNA
Sorption
Desorption
Enzymatic degradation

ABSTRACT

With increasing environmental application, biochar (BC) will inevitably interact with and impact environmental behaviors of widely distributed extracellular DNA (eDNA), which however still remains to be studied. Herein, the adsorption/desorption and the degradation by nucleases of eDNA on three aromatized BCs pyrolyzed at 700 °C were firstly investigated. The results show that the eDNA was irreversibly adsorbed by aromatized BCs and the pseudo-second-order and Freundlich models accurately described the adsorption process. Increasing solution ionic strength or decreasing pH below 5.0 significantly increased the eDNA adsorption on BCs. However, increasing pH from 5.0 to 10.0 faintly decreased eDNA adsorption. Electrostatic interaction, Ca ion bridge interaction, and π-π interaction between eDNA and BC could dominate the eDNA adsorption, while ligand exchange and hydrophobic interactions were minor contributors. The presence of BCs provided a certain protection to eDNA against degradation by DNase I. BC-bound eDNA could be partly degraded by nuclease, while BC-bound nuclease completely lost its degradability. These findings are of fundamental significance for the potential application of biochar in eDNA dissemination management and evaluating the environmental fate of eDNA.

Introduction

Extracellular deoxyribonucleic acid (eDNA) excreted by microorganisms, plants, and animals including dying cells plays an important role in biological heredity and variation, ecological and genetic diversity, and biological evolution (Ochman et al., 2000). eDNA is widely distributed in the environment, reaching 0.03–200 μg/g in soil and 0.2–44 μg/L in aquatic environments (Pietramellara et al., 2009). Moreover, eDNA is recognized to be a carrier of antibiotic resistance genes (ARGs) that are classified as a type of emerging pollutant and pose threat to public health (WHO, 2015). Investigations show that the concentration of ARGs in eDNA (eARGs)

* Corresponding author.
E-mail: lindaohui@zju.edu.cn (D. Lin).

https://doi.org/10.1016/j.jes.2020.08.017
1001-0742/

in sediments and effluents of sewage treatment plants is significantly higher than that of ARGs in intracellular DNA (Mao et al., 2014; Zhang et al., 2018a). eDNA can be taken by various bacteria for genetic recombination and genetic transformation in horizontal gene transfer (HGT), which may contribute to the dissemination of ARGs in the environment (Zhang et al., 2018a). Therefore, it is essential to explore the environmental behavior of eDNA.

Biochar (BC), a type of carbon material obtained from biomass pyrolysis under anaerobic or anoxic conditions, has been increasingly applied in agricultural and environmental remediation domains (Ahmad et al., 2014; Wang et al., 2013; Lian and Xing, 2017). With increasing amount of BC added into the environment, predicting the magnitude of eDNA sorption onto BC and identifying the controlling sorption domains became important and urgent for assessing the fate and risk associated with eDNA. However, our current information on the sorption of eDNA with BC are rather limited. Wang et al. (2014) observed that eDNA adsorption capacity of willow wood BC generally increased with pyrolysis temperature (300–600 °C), and the specific surface area and micropore surface area were considered as the main factors influencing eDNA adsorption. But the underlying sorption mechanisms were not specifically addressed. Other studies have investigated the effect of BC on the extraction of eDNA from soil using PowerSoil® DNA Isolation Kit (Jin, 2010; Hale and Crowley, 2015; Dai et al., 2017). Hale and Crowley (2015) found addition of four types of BCs (from palm fronds, pinewood, coconut, and pistachio nut shells) did not reduce the efficiency of DNA extraction compared to unamended soils. In contrast, the eDNA extraction rate from soil significantly decreased in the presence of corn-stover BC (Jin, 2010) and high-ash BC from autoclaved swine manure (Dai et al., 2017). These contradictory results are probably attributed to complex properties of BCs. It is well-known that the composition and functional groups of BCs are highly dependent on the feedstock and pyrolytic temperature (Keiluweit et al., 2010). With increasing pyrolysis temperature to higher than 700 °C, the amorphous aliphatic domain in BC evolves into the condensed aromatic moiety comprised of graphitic sheets and rich in pores during pyrolysis, and finally generates aromatized BC (Keiluweit et al., 2010; Zhang et al., 2018b). It has been reported that aromatized BC has higher adsorption affinity than those of non-aromatized BC to organic pollutants containing aromatic structures (Chen et al., 2008, 2012; Rajapaksha et al., 2014; Uchimiya et al., 2010; Yang et al., 2018; Zhang et al., 2018b). Several mechanisms may contribute to sorption of eDNA onto BC, including electrostatic interaction, hydrophobic interactions, ligand exchange between eDNA and hydroxyl (-OH) groups of BCs, cation bridging between eDNA and negatively charged functional groups of BCs, and π-π interaction between eDNA and the aromatic surface of BC. The exact mechanism and its impacting factors of eDNA-BC interaction warrant more investigation.

Many studies confirmed that the adsorption of eDNA on solid particles resulted in the protection of eDNA against enzymatic degradation, but the protection mechanism still remains controversial (Khanna and Stotzky, 1992; Demaneche et al., 2001; Cai et al., 2006a,b, 2008; Yang et al., 2012). Some studies proposed that the binding of eDNA on adsorbents altered the conformation and electron distribution of eDNA, which prevented nuclease from recognizing or interacting with appropriate cleavage sites (Stotzky, 2000; Cai et al., 2008). In contrast, other studies reported that the protection of eDNA against nuclease degradation by clay minerals and soil colloids was apparently not controlled by the adsorption affinity of eDNA molecules and the conformation change of bound eDNA, but correlated to the adsorption affinity of nucleases on adsorbents due to inactivation of enzyme activity (Cai et al., 2006a, 2007; Khanna and Stotzky, 1992). These contradictory results indicate the protection of eDNA by adsorption behavior varied significantly with the adsorbents. However, information on the protection of eDNA by BC and the mechanisms is still lack by so far. Such information is essential to understand the persistence of eDNA in BC amended soils.

Therefore, the objectives of the current research were to: (1) investigate the adsorption/desorption behaviors and mechanisms of eDNA on three aromatized BCs pyrolyzed at 700 °C from three types of high yield agricultural waste biomass including wood chips, wheat straw, and peanut shells; (2) examine the level of protection of eDNA by BCs against nuclease degradation and the protection mechanisms. The adsorption kinetics, adsorption/desorption isotherms, and the effects of solution chemistry, i.e., ionic strength (IS), ion composition (Na^+ or Ca^{2+}), and pH, on the adsorption of eDNA by BCs were systematically investigated. The protection mechanisms of eDNA by BCs from nuclease degradation were discussed from two aspects, i.e., whether the BC-bound eDNA could be degraded by free nuclease and whether the free eDNA could be degraded by BC-bound nuclease. This work will be helpful for better understanding the potential interactions between eDNA and BC in the environment.

1. Materials and methods

1.1. *eDNA and DNase I*

Salmon sperm eDNA was purchased from Sigma Chemical (Co., St. Louis, MO, USA). The purity of eDNA was assessed by the UV light absorbance at 260 and 280 nm (A_{260}/A_{280} ratio >1.8) (Wang et al., 2014). Bovine pancreas DNase I was obtained from Roche Diagnostics GmbH Mannheim, Germany. Other chemicals including Tris buffer ($NH_2C(CH_2OH)_3$), NaCl, $CaCl_2$, $NaH_2(PO_4)_3$, and NaOH with reagent grade were purchased from Sigma.

1.2. *Preparation and characterization of BCs*

The pre-washed and pre-dried (80 °C) local wood chip, wheat straw, and peanut shell were carbonized under anoxic conditions in a muffle furnace (SX2-12-10, Jinan Precision Scientific Instruments Co., China) with a heating rate of 5 °C/min to the target pyrolysis temperature of 700 °C which was then maintained for 6 hr. The resultant BCs from wood chip, wheat straw, and peanut shell were labeled as WC700, WS700, and PS700, respectively. The BCs were ground and sieved (75 μm). All obtained BC samples were stored in air tight containers in a desiccator prior to use.

Multiple instruments were used to characterize physicochemical properties of the three BC samples. The pH of BCs in ultrapure water (1:50, *M/V*) was measured with a pH meter. Total C, H, and N contents were measured using an elemental analyzer (MicroCube, Elementar, Germany) and the O content was determined by the mass balance calculation as previously reported (Chen et al., 2008). The ash content was determined by a thermogravimetric analyzer (TGA, SDTA851, Swrtzer Land, America). The Brunauer–Emmett–Teller (BET) surface area analysis was conducted on a Quantachrome, AUTO-SORB AS-1 surface area analyzer (Micromeritics Instrument Co. Ltd., USA). The surface functional groups were analyzed by Fourier transform infrared spectroscopy (FTIR, Tensor 27, Bruker Optics, Germany). The zeta potentials of BCs in various solutions were measured by using a Zetasizer (Nano ZS90, Malvern Instrument Ltd., UK).

1.3. *Batch experiments for eDNA adsorption and desorption*

Kinetic adsorption experiments were carried out at 25±1 °C. Fifty milligrams of BCs were mixed into 10 mL of Tris buffer (10 mmol/L) containing 50 mg/L eDNA and 100 mmol/L NaCl in 10-mL polyethylene centrifuge tubes. The mixture was shaken on a vertical motion (KS 130 B S25, IKA, German) at 720 r/min for different time (5 min, 10 min, 20 min, 40 min, 90 min, 4 hr, 8 hr, 1 day, 2 day, 3 day, 4 day, 5 day, or 6 day), followed by centrifugation at 13,000 r/min for 5 min. The eDNA concentration in the supernatants was determined by the absorbance at 260 nm (Wang et al., 2014). Control reactors, prepared identically but containing no eDNA, were simultaneously run to assess the effect of dissolved organic carbon (DOC) from BC on the determination of eDNA at 260 nm. The preliminary experiment showed that the absorbances at 260 nm of filtrates from WC700, WS700, and PS700 were all lower than 0.03 and the absorbance of 50 mg/L eDNA was around 0.82, indicating the effect of DOC from BCs on eDNA detection could be reasonably deducted. The preliminary experiments also showed that the microbial degradation or uptake to the glass walls of eDNA were negligible during 10 days' incubation. Adsorption and desorption isotherm experiments were the same as kinetic experiments except that different concentrations of eDNA were used and the equilibration time was 4 days. The effect of solution IS on eDNA adsorption was investigated in the presence of 10–100 mmol/L Na^+ (NaCl) or 5–25 mmol/L Ca^{2+} ($CaCl_2$). To evaluate the influence of pH, an experiment with 80 mg/L eDNA in 100 mmol/L NaCl solution was conducted at pH 3–10 adjusted by 0.01 mol/L HCl or 0.01 mol/L NaOH. Desorption experiments of eDNA were conducted in sequential decant-refill steps immediately following the completion of the adsorption experiments. Supernatant (8 mL) was removed by a pipette and immediately replaced by the same volume of corresponding background solution and the vials were resealed and shaken for an additional 4 days. After 4 days' equilibration, eDNA in the supernatant was determined and the amount of eDNA desorbed was calculated by the mass difference. Hysteresis index (HI) was calculated to evaluate the irreversibility of adsorption (Sander et al., 2005). The desorption of eDNA from BCs was also conducted by using 0.1 mol/L sodium phosphate buffer (pH 6.0) or 1% sodium dodecyl sulfate (SDS) solution at an initial eDNA concentration of 100 mg/L. All experiments were conducted in duplicate. In addition, the adsorption kinetics of eDNA on BCs were fitted by pseudo-second-order kinetic model (Azizian, 2004; Önal, 2006). The adsorption isotherms were fitted by both Langmuir and Freundlich isotherm models (Allen et al., 2004). The pseudo-second-order kinetic model, Langmuir and Freundlich isotherm models, and the calculation method of HI are detailed in Appendix A (Text S1-S3).

1.4. *Spectral measurements*

FT-IR spectra of eDNA, BCs, and eDNA-BC complexes were obtained on a FT-IR spectroscopy (Tensor 27, Bruker Optics, Germany). Solid salmon sperm eDNA and BCs were used directly to obtain FT-IR spectra. The eDNA-BC complexes were prepared by reacting 2 mg of eDNA with 50 mg of BC particles in 10 mL of 10 mmol/L Tris buffer. After the shaking and centrifugation processes, the precipitate was washed four times with 1 mL of 10 mmol/L Tris buffer (pH 7.0) to remove any weakly associated eDNA. After being freezingly dried, the eDNA-BC complexes were used for the FT-IR analysis. Circular dichroism (CD) spectra of the pristine eDNA dissolved in 10 mmol/L Tris buffer, the pristine eDNA in 100 mmol/L NaOH, and the eDNA desorbed with 100 mmol/L NaOH from BCs were recorded with a J-810 spectropolarimeter (Jasco Japan) and subtracted from the spectrum of buffer alone. NaOH may facilitate the desorption of eDNA that was hard to be desorbed by background adsorption solution (Hou et al., 2014). Each measurement included three repeated scans, and the average CD signal was converted to ellipticity.

1.5. *Degradation of eDNA in the absence and presence of BCs*

The degradation behavior of eDNA by DNase I was investigated in three scenarios: (1) simple multiple mixture of BCs, eDNA, and DNase I; (2) binary mixture of BC-bound eDNA and free DNase I; (3) binary mixture of free eDNA and BC-bound DNase I. For scenario (1), 25 or 50 mg of BCs were mixed with 5 mL of 10 mmol/L Tris buffer (pH 7.0) containing 500 μg of eDNA in a centrifuge tube. The mixture was gently shaken (at 150 r/min) at 25 °C for 1 hr, and 1 mL of DNase I solution was then added to the suspension to yield final nuclease concentrations ranging from 0 to 6.4 μg/mL. The mixture was incubated at 25 °C for 1 h, and then 5 μL of the suspension was analyzed using 1% agarose gel electrophoresis which was run for 35 min at 110 V at 25 °C. The gels were photographed with an UVP gel scanner. For scenario (2), both UV–vis and agarose electrophoresis analyses were conducted for the degradation of BC-bound eDNA by pristine DNase I. To obtain BC-bound eDNA, 25 mg of BCs were mixed with 5 mL of 10 mmol/L Tris buffer (pH 7.0) containing 500 μg of eDNA in a centrifuge tube. Then the mixture was gently shaken (at 150 r/min) at 25 °C for 2 hr and centrifuged at 13,000 r/min for 5 min. Then the supernatant was removed and 5 mL of 6.4 μg/mL DNase I were added in the precipitated mixture and incubated at 25 °C for 1 hr. Finally, the suspension was tested by the UV–vis and agarose electrophoresis analyses with the same steps as above

Table 1 – Selected physicochemical properties of the three BCs.

BC types	pH	Ash (%)	C (%)	H (%)	O (%)	N (%)	H/C	O/C	(O+N)/C	SSA (m^2/g)	A_{micro} (m^2/g)	A_{exter} (m^2/g)	A_{micro}%	D (nm)
WC700	6.8	2.0	76.8	2.5	18.5	0.2	0.39	0.18	0.183	493	338	155	68.6	28
WS700	10.7	18.7	67.3	1.5	11.8	0.7	0.27	0.13	0.140	341	262	78.7	76.9	21
PS700	10.3	6.4	81.7	2.3	8.7	0.8	0.34	0.08	0.088	241	184	57.2	76.3	20

WC700, WS700 and PS700 represents the biochar from wood chip, wheat straw and peanut shell at pyrolysis temperature of 700°C, respectively. SSA denotes specific surface area, A_{micro} denotes micropore area, A_{exter} denotes external surface area, A_{micro}% denotes the percentage of A_{micro} in SSA, and *D* denotes average pore size of biochar.

to monitor eDNA. Preliminary experiment showed that the absorbance of 6.4 μg/mL DNase I was lower than 0.001 at 260 nm, indicating the effect of DNase I on eDNA determination was negligible. For scenario (3), agarose electrophoresis analysis was conducted for the degradation of free eDNA by BC-bound DNase I. To obtain BC-bound DNase I, 25 mg of BCs were mixed with 5 mL of 6.4 μg/mL DNase I in a centrifuge tube, then the mixture was gently shaken at 25 °C for 2 hr and centrifuged at 13,000 r/min for 5 min. Then the supernatant was removed and 5 mL of 10 mmol/L Tris buffer (pH 7.0) containing 500 μg of eDNA were added in the precipitated mixture and incubated at 25 °C for 1 hr. Finally, the suspension was tested by agarose electrophoresis with the same steps as above. The degradation of pristine eDNA in the absence of BCs was also measured as the control.

The adsorption of DNase I on BCs was also conducted. Five milligrams of BCs were mixed with 3.5 mL of deionized water containing 200 μg/mL DNase I. The mixture was gently shaken (at 150 r/min) at 25 °C for 1 hr and centrifuged at 13,000 r/min for 5 min. DNase I in the supernatant was determined at 280 nm (Cai et al., 2006a). The amount of DNase I adsorbed was calculated by the mass difference.

1.6. *Statistical analysis*

All experimental data were expressed as the mean of two independent determinations. The significance of differences was analyzed using a one-way ANOVA with a least significant difference test ($p<0.05$).

2. Results and discussion

2.1. *Characteristics of BC*

The pHs, elemental compositions, atomic ratios, and specific surface areas of BCs are listed in Table 1. The pHs of WC700, WS700, and PS700 were 6.8, 10.7, and 10.3, respectively. The ash contents deceased in the order of WS700 (18.7%) > PS700 (6.4%) > WC700 (2.0%), consistent with previous studies that ash content was higher in BC from agriculture straw than those from wood (Han et al., 2018; Song et al., 2019). The specific surface areas decreased in the order of WC700 (493 m^2/g) > WS700 (341 m^2/g) > PS700 (241 m^2/g), the same as the order of their micropore areas and external surface areas (Table 1). High content of carbon (> 67%) was fixed in BCs with pyrolysis temperature of 700 °C in this study, reflecting the highly condensed and thermally stable C components. WC700 had the highest molar ratio of H/C (0.39), followed by PS700 (0.34) and WS700 (0.27), indicating the condensation degree of aromatic carbon in BCs increased in turn. A H/C ratio of 0.3 represents substances having a very highly condensed aromatic ring system (Hammes et al., 2006; Qian et al., 2016). The polarity indexes of O/C and (O+N)/C are commonly used to indicate the abundance of polar functional groups (Chen et al., 2008; Lin et al., 2007). PS700 had the lowest ratios of O/C and (O+N)/C, indicating the lowest content of oxygen functional groups, while WC700 had the highest polar functional groups with the highest O/C ratio.

The FTIR spectra of BCs are illustrated in Fig. 1. All BCs exhibited peaks at 1145–1100 cm^{-1} and 885 cm^{-1}, which are assigned to the C–O–C and C–C stretching in aromatic cores (Chen et al., 2008) and to the C–H stretching of aromatic rings (Keiluweit et al., 2010), respectively. This result confirmed that BC pyrolyzed at 700 °C had high aromatic surface. Remarkably, the sharp peaks at around 1400 cm^{-1} and 1573 cm^{-1}, attributing to the C–OH (Peng et al., 2016) and aromatic C=C stretching (Li et al., 2014; Lin et al., 2007), respectively, were found in the three BCs, indicating the presence of phenolic hydroxyl groups. In addition, WC700 had a peak at around 1700 cm^{-1}, indicating the presence of C=O (Nguyen and Lehmann, 2009), which was not observed for WS700 and PS700. WS700 had a peak at 467 cm^{-1} representing Si–O–Si stretching (Xiao et al., 2014). Wheat is a typical silicon-accumulating plant (Ma and Takahashi, 2002), thus resulting in the accumulation of Si in WS700.

2.2. *Adsorption kinetics of eDNA on BCs*

The adsorption kinetics plots of eDNA on BCs and their kinetic modelling plots are depicted in Fig. 2. The related kinetic parameters and correlation coefficients (R^2) are presented in Appendix A Table S1. Depending on BC types, eDNA adsorption reached an equilibrium within 1 to 3 days at 25 °C, which is much longer than the equilibrium time of eDNA on soils, minerals, and humic acids (1-3 hr) (Cai et al., 2006a, 2007; Saeki et al., 2011). As shown in Fig. 2b and Appendix A Table S1, the pseudo-second-order model well fitted the eDNA adsorption kinetics on BCs with high R^2 (0.999). The rate constant (k_2) of WC700 (64.0 g/mg/day) was more than 18 times higher than that of WS700 (3.5 g/mg/day) and PS700 (2.9 g/mg/day), suggesting that WC700 had the fastest adsorption. Similar trend was also found in the early stage of the adsorption as inferred from the initial rate of adsorption parameter (*h*).

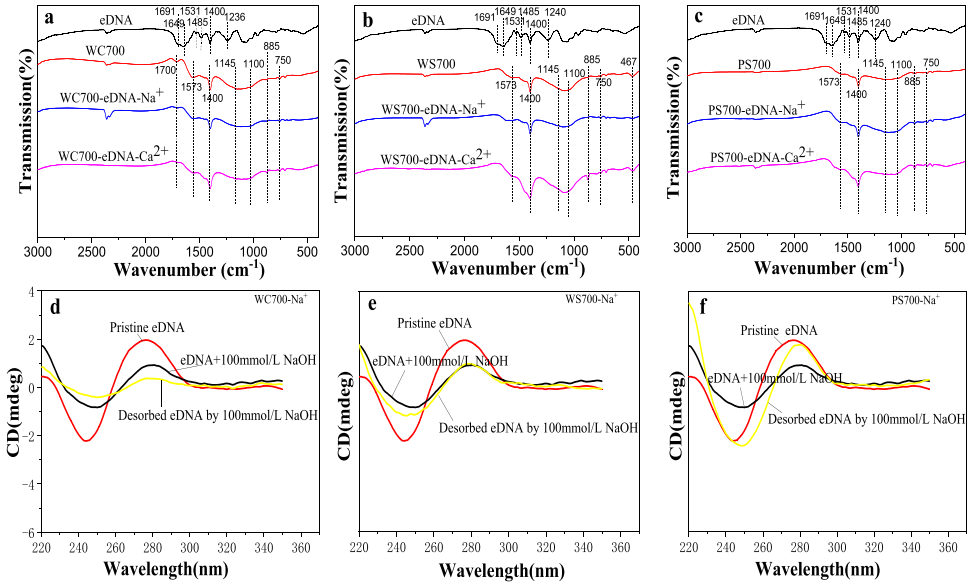

Fig. 1 – Fourier transform infrared spectroscopy (FTIR) and circular dichroism (CD) spectra analysis for BCs and eDNA. a–c: FTIR spectra of eDNA, BCs, and BCs bound eDNA complexes in NaCl and $CaCl_2$ solutions. d–f: CD spectra of pristine eDNA, free eDNA in 100 mmol/L NaOH, eDNA desorbed by 100 mmol/L NaOH solutions from BCs.

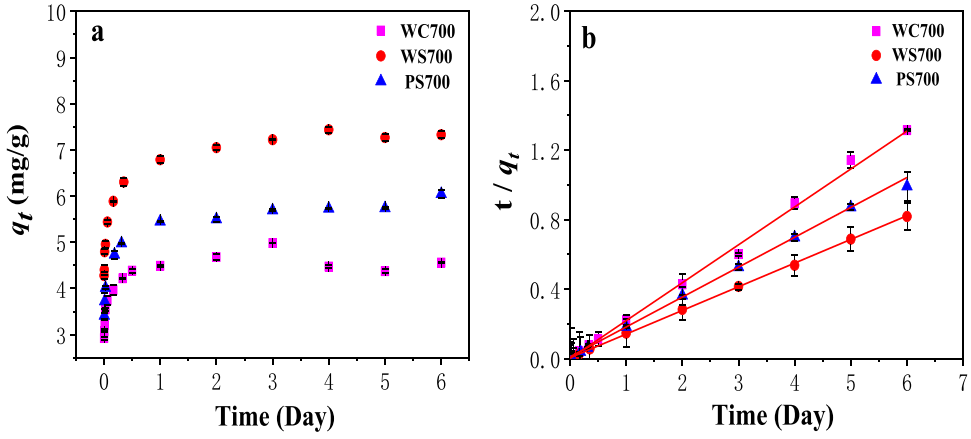

Fig. 2 – Sorption kinetics of eDNA on BCs (a) and the corresponding modelling plots by pseudo-second-order kinetic model (b) under IS=100 mmol/L NaCl.

In general, the adsorption process involves multisteps, mainly including the external surface mass transfer (boundary layer diffusion) and the subsequent intraparticle diffusion (Porkodi and Vasanth Kumar, 2007; Cáceres-Jensen et al., 2013). The highest adsorption rate of WC700 indicated that WC700 surface had the weakest resistance to mass transfer of eDNA in the external liquid and the fastest intraparticle diffusion, probably due to the largest external surface area and pore size (Table 1). Following the external surface mass transfer step, the intraparticle diffusion, i.e., eDNA molecules diffusing slowly into pores of BC starts controlling the rate of adsorption until the equilibrium plateau is reached. The larger percentage of micropore areas in SSA of WS700 (76.9%) and PS700 (76.3%) could be responsible for their slower adsorption kinetic rates.

2.3. *Adsorption and desorption of eDNA on BCs*

2.3.1. *Adsorption isotherms of eDNA on BCs*

The adsorption isotherms of eDNA on BCs are presented in Fig. 3a–c (solid labels) and the fitted parameters of Langmuir and Freundlich models are listed in Table 2. The Freundlich model generally fitted the adsorption data better than the Langmuir model as indicated by the higher R^2 of the former fitting (Table 2). Both the Freundlich affinity coefficient (K_F) and a single-point adsorption coefficient K_d values (at C_e=10 mg/L) were in the order of WS700 > PS700 > WC700 at a same solution chemistry. The values of nonlinearity indicator N were less than 0.3, indicating a wider adsorption site energy distribution on BC (Fang et al., 2008). Formation of aromatic and condensed structures in BCs at high pyrolysis temperature

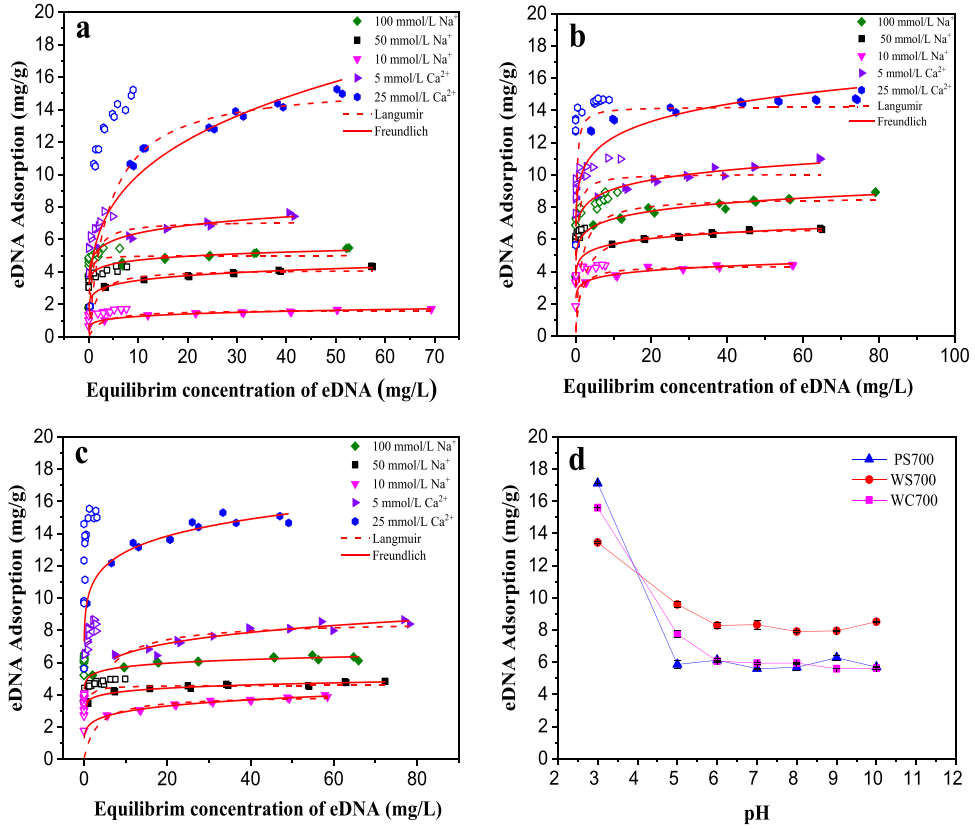

Fig. 3 – Sorption and desorption isotherms of eDNA on (a) WC700, (b) WS700, and (c) PS700) under different solution IS; (d) the adsorption of eDNA on BCs at various solution pHs and 50 mg/L eDNA (IS=100 mmol/L NaCl). Solid labels are adsorption data, and hollow labels with the same shape are the corresponding desorption data.

would generate significant heterogeneous surface energy distribution of BC (Zheng et al., 2013). Fig. 3 shows that the adsorption of eDNA on BCs increased markedly with increasing NaCl concentration from 10 mmol/L to 100 mmol/L. The K_d values (at C_e=10 mg/L) of WC700, WS700, and PS700 increased by 3.75, 1.91, and 1.94 times, respectively, when NaCl increased from 10 to 100 mmol/L (Table 2). The adsorption of eDNA on inorganic clay and kaolinite also increased with increasing NaCl concentration (Cai et al., 2006a, Saeki et al., 2010). However, Wang et al. (2014) found the addition of NaCl (0.2–60 mmol/L) had no significant effect ($p>0.05$) or even inhibited the adsorption of eDNA on willow wood BC, due to the replacement of BC surface-attached Ca^{2+} and Mg^{2+} ions by Na^+. Considering the isoelectric point of eDNA at pH 5.0 (Wang et al., 2014) and the negative zeta potential values of BCs (Appendix A Fig. S2a), both eDNA molecules and BCs had negative charges in the adsorptive systems (pH > 6.7) in this study. Cations can neutralize negative charges on the surfaces of BCs and thus increase the eDNA adsorption. The zeta potentials of BCs significantly decreased with increasing Na^+ or Ca^{2+} concentrations (Appendix A Fig. S2a), indicating the electrostatic repulsion between eDNA and BC decreased and thus the eDNA adsorption increased correspondingly. The charge screening effect of Ca^{2+} could be much stronger than that of Na^+ as indicated by the surface electronegativity in Ca^{2+} solutions (Appendix A Fig. S2a), which may explain the much greater adsorption of eDNA in the presence of Ca^{2+} than Na^+ (Fig. 3). Furthermore, in comparison with Na^+, Ca^{2+} could likely form ion bridge between the phosphate groups of eDNA and acidic groups (e.g., carboxyl and phenolic groups) on the adsorbent surfaces (Cai et al., 2006a; Nguyen and Chen, 2007), and thereby also increase the adsorption. The Ca^{2+} bridge between the phosphate groups of eDNA and BC surfaces was evidenced by FTIR analysis (Fig. 1a–c). The band at around 1400 cm^{-1} representing the C-OH stretching in BCs (Peng et al., 2016) became wider in Ca^{2+} systems, which may prove the existence of Ca^{2+} bridge between $C–O^-$ and the phosphate groups of eDNA.

The influence of pH on eDNA adsorption by BCs was also investigated. As shown in Fig. 3d, the amounts of eDNA adsorbed by WC700, WS700, and PS700 deceased from 15.6 to 7.7, 13.4 to 7.6, and 17.1 to 5.9 mg/g, respectively, with increasing pH from 3.0 to 5.0. The eDNA molecule was protonated and positively charged at pH 3.0 (below the isoelectric point of eDNA, i.e., 5.0) (Cai et al., 2006a; Wang et al., 2014), while BC surfaces were still negatively charged at this pH (Appendix A Fig. S2b). Electrostatic attraction could thus occur and contribute to the high adsorption of eDNA at pH 3.0. The electronegativity of BC significantly increased with increasing pH from 5.0 to 10.0 (Appendix A Fig. S2b), and thus the electrostatic repulsion between eDNA and BCs would increase. However, the eDNA adsorption on aromatized BC kept largely unchanged within pH 5.0–10.0 (Fig. 3d), suggesting that other

Table 2 – Langmuir and Freundlich models-fitted parameters for eDNA adsorption on BCs.

BC types	Solution IS	Langmuir model			Freundlich model			
		Q_{max} (mg/g)	K_L (L/mg)	R^2	K_F (mg/g)/(mg/L)^N	N	R^2	K_d (L/g)
WC700	10 mmol/L Na^+	1.67	0.42	0.90	0.86	0.16	0.97	0.13
	50 mmol/L Na^+	4.15	0.77	0.80	2.64	0.12	0.98	0.35
	100 mmol/L Na^+	5.01	9.44	0.66	4.00	0.07	0.95	0.47
	5 mmol/L Ca^{2+}	7.13	1.53	0.72	5.01	0.10	0.95	0.64
	25 mmol/L Ca^{2+}	15.7	0.25	0.99	5.18	0.28	0.94	0.10
WS700	10 mmol/L Na^+	4.37	1.10	0.83	3.07	0.09	0.88	0.38
	50 mmol/L Na^+	6.75	0.51	0.90	4.70	0.08	0.97	0.57
	100 mmol/L Na^+	8.60	0.71	0.77	5.90	0.09	0.95	0.73
	5 mmol/L Ca^{2+}	10.1	3.09	0.63	7.45	0.09	0.96	0.91
	25 mmol/L Ca^{2+}	14.2	5.84	0.90	9.54	0.11	0.87	1.23
PS700	10 mmol/L Na^+	3.97	0.33	0.88	2.04	0.16	0.98	0.30
	50 mmol/L Na^+	4.60	4.06	0.75	3.62	0.07	0.94	0.42
	100 mmol/L Na^+	—	—	—	5.05	0.06	0.92	0.57
	5 mmol/L Ca^{2+}	8.58	0.32	0.77	4.84	0.13	0.89	0.66
	25 mmol/L Ca^{2+}	—	—	—	10.1	0.11	0.95	1.29

WC700, WS700 and PS700 represents the biochar from wood chip, wheat straw and peanut shell at pyrolysis temperature of 700 °C, respectively. "—" denotes failed fitting; the single-point adsorption coefficient K_d was calculated at C_e = 10 mg/L according to the Freundlich model.

mechanisms besides the electrostatic interaction could dominate the interactions between eDNA and aromatized BC at pH > 5.0.

2.3.2. *π-π interactions between eDNA and aromatized BCs*

Many studies suggest that eDNA could adsorb on carbon-based nanoparticles (e.g., graphene, carbon nanotubes, and C_{60}) through π-π interactions between eDNA bases and the sp2-hybridised carbon rings of aromatic carbon in aqueous environments (Zhao, 2011; Roxbury et al., 2010; Ahmed et al., 2012; Zeng et al., 2015; Sun et al., 2017). Similar as graphitic materials, e.g., graphene and carbon nanotubes, aromatized BCs in this study had high aromatic domains with low H/C (Table 1). Therefore, the existence of strong π-π interactions between eDNA and aromatic carbon of BC is expected. This speculation was confirmed by the FTIR analysis. As shown in Fig. 1a–c, The main absorption bands of salmon sperm eDNA included: 1236 cm^{-1} corresponding to the antisymmetric stretching vibration of the phosphate group, 1400 cm^{-1} of base moieties, 1485 cm^{-1} of cytosine, 1531 cm^{-1} of imidazole ring, 1649 cm^{-1} of C=C and C=N stretching in the base planes, and 1691 cm^{-1} of the C=O stretching in guanine (Cai et al., 2006a; Oliveira et al., 2019; Sheng et al., 2019). The antisymmetric PO_2^{-1} stretching band is a characteristic marker for eDNA backbone conformation and the band at 1236 cm^{-1} suggests the eDNA remained in a B-conformation (Mady et al., 2011). No new peaks were observed for BC-eDNA complexes, probably due to the low amount (< 16 mg/g, Fig. 3a–c) of adsorbed eDNA that could not be detected. However, the peak corresponding to skeletal vibration of aromatic C=C of BCs bonds (around 1573 cm^{-1}) decreased in intensity and upshifted after eDNA adsorption (i.e. from 1573 cm^{-1} to 1618 cm^{-1} on WS700 in NaCl solution), indicating the presence of π-π interactions between BC and eDNA bases. This is in good agreement with the observation of Tran et al. (2017). They concluded that π-π interactions existed between the benzene rings of methylene green and aromatic carbon of activated charcoal after observing an upshift of the C=C bond peak from 1537 cm^{-1} to 1561 cm^{-1} upon methylene green adsorption on activated charcoal.

2.3.3. *Desorption of eDNA from BCs*

The desorption isotherms of eDNA from BCs under different solution chemistry are presented in Fig. 3a–c (hollow labels). Remarkably, the desorption isotherm of eDNA on BC is significantly above the adsorption isotherm, indicating the irreversible adsorption. Desorption hysteresis is conceptually considered to be a result of pollutant irreversibly bound to sorbents (Fang et al., 2008; Adamson, 1990; Rojas et al., 2001; Wu et al., 2013). Hysteresis index (HI) can be used to determine the irreversibility of adsorption, which is based on the difference in free energy between the real desorption state and the hypothetical fully reversible state (Sander et al. 2005). The HI is 0 for completely reversible systems and approaches 1 as the process tends toward complete irreversibility. The desorption of eDNA from aromatized BC in the Tris-NaCl solution (sorption background electrolyte solution) was negligible with HI values close to 1 (Appendix A Table S2), indicating the completely irreversible adsorption of eDNA on the aromatized BCs. In order to better understand mechanisms involved in the eDNA adsorption by BCs, the desorption of eDNA by 0.1 mol/L NaH_2PO_4 or 1% SDS was also conducted, which indicated the ligand exchange and hydrophobic interactions, respectively (Saeki et al., 2011). As shown in Appendix A Table S3, the desorption rates by either NaH_2PO_4 or SDS were all very low (<2%), indicating that few eDNA molecules on aromatized BC were bound by ligand exchange or hydrophobic interactions.

2.3.4. *Conformational changes of eDNA before and after adsorption*

CD spectra can be used to analyze conformation transition of eDNA (Zhou et al., 2004; Banyay et al., 2002; Cai et al., 2006a). Fig. 1d–f and Appendix A Fig. S3 show the CD spectra of the pristine eDNA and the desorbed eDNA from BC by NaOH. The CD spectrum of pristine eDNA was observed a typical B-form

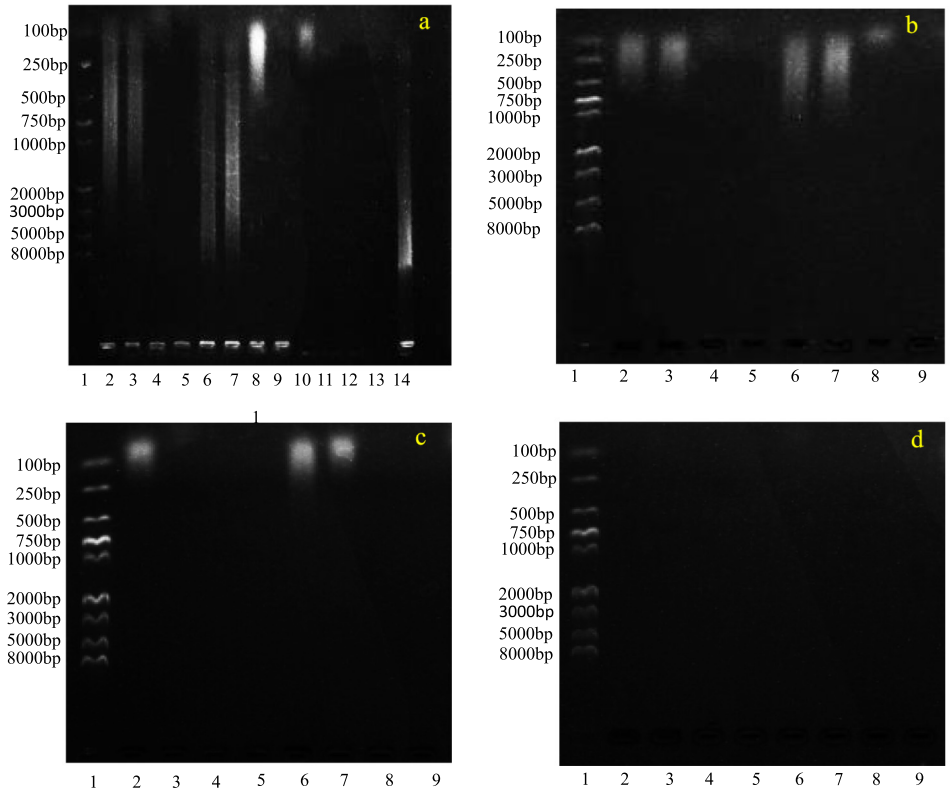

Fig. 4 – Agarose electrophoresis of the degradation of free eDNA (a) and eDNA with kaolinite (a), WC700 (b), PS700 (c), and WS700 (d) by various concentrations of DNase I. Lane1:Trans2K® Plus II DNA Marker; Lanes 2–5: 0.8, 1.6, 3.2, and 6.4 μg of DNase I/mL at the solid to liquid ratio of 1: 200; Lanes 6–9: 0.8, 1.6, 3.2, and 6.4 μg of DNase I/mL at the solid to liquid ratio of 1: 100; and Lanes 10–14 in (a): 0.8, 1.6, 3.2, 6.4, and 0 μg of DNase I/mL in the absence of solid adsorbents.

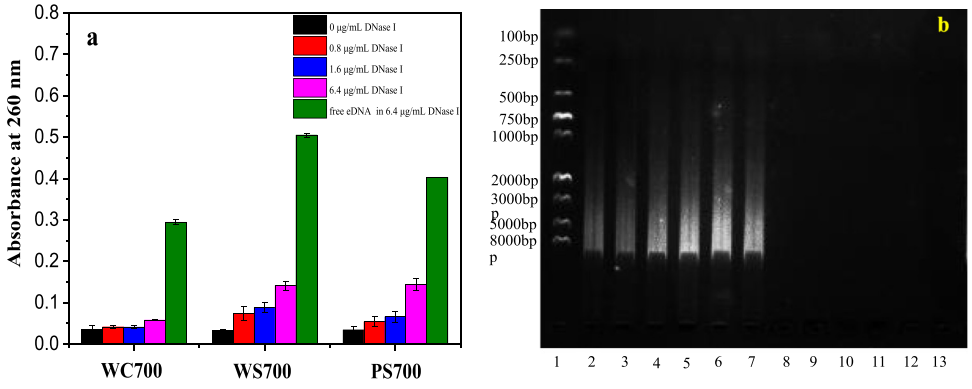

Fig. 5 – The UV–vis and agarose electrophoresis analyses for the degradation of BC-bounded eDNA by DNase I and free eDNA by BC-bounded DNase I. (a) the UV–vis absorbance of the degradation solution at 260 nm for BC-bounded eDNA and free eDNA (the same amount to corresponding adsorbed eDNA on BC) by various concentrations of DNase I. (b) agarose electrophoresis of the degradation of free eDNA (100 mg/L) by BC-bounded DNase I (Lanes 2–7) and the degradation of BC-bounded eDNA by free DNase I (6.4 μg/mL) (Lanes 8–13) in the presence of BCs with a solid to liquid ratio of 1:200. Lane1: Trans2K®Plus II DNA Marker; Lanes 2–3 and 8–9: with WC700; Lanes 4–5 and 10–11: with WS700; Lanes 6–7 and 12–13: with PS700.

(Sun et al., 2002), exhibiting a positive band at 276 nm and a negative band at 244 nm in the Tris-NaCl solution or a positive band at 278 nm and a negative band at 245 nm in the Tris-$CaCl_2$ solution. The typical C-form, A-form, and Z-form of DNA have positive bands at 296 nm, 260 nm, and 260 nm, and corresponding negative bands at 248 nm, 210 nm, and 290 nm, respectively (Heller et al., 2006; Kypr et al., 2009). Although both the positive and negative bands of the CD spectrum of free eDNA in NaOH solution were red shifted, the variation range was less than 5 nm, indicating eDNA conformation was not affected by the desorption agent (NaOH) in this work. In NaCl systems, the eDNA molecules desorbed from WC700, WS700, and PS700 had CD peaks at 277 nm, 279 nm, and 280 nm, and the corresponding negative valleys at 250, 245, and 249 nm, respectively, which were similar to the pristine eDNA and free eDNA in NaOH solution, suggesting that eDNA desorbed from BC retained most of its original B-form structure. Similar results were also observed in $CaCl_2$ systems (Appendix A Fig. S3). The eDNA conformation of B-form did not changed by the sorption on aromatized BC in this study.

2.4. *Degradation of eDNA by DNase I with and without BCs*

Electrophoresis of free eDNA and eDNA in the simple multiple mixture of BC, eDNA, and DNase I (scenario 1) are shown in Fig. 4. The pristine eDNA mainly contained fragments within 1000–8000 bp in the absence of DNase I (Fig. 4a, lane 14), and it was degraded to smaller than 250 bp segments in the presence of 0.8 μg/mL DNase I (Fig. 4a, lane 10). When the concentration of DNase I increased to 1.6 μg/mL or higher, the pristine eDNA was entirely degraded (no eDNA band) (Fig. 4a, lane 11). Compared with the free eDNA, no obvious change was observed in the electrophoresis pattern of eDNA in suspensions of BC in the absence of DNase I (Appendix A Fig. S4), indicating that the structure of eDNA was not affected by the presence of BC. As shown in Fig. 4b and c, in systems of WC700 and PS700 with a solid to water ratio of 1:100, eDNA was degraded to <1000 bp and <250 bp segments by 1.6 μg/mL DNase I (lane 7), respectively. When increasing DNase I to 3.2 μg/mL, eDNA was degraded to around 100 bp segments in the presence of WC700 (Fig. 4b, lane 8), while it was completely degraded with PS700 (Fig. 4c, lane 8). These results indicate that both WC700 and PS700 could provide a certain protection for eDNA from degradation by the nuclease, and WC700 could provide more protection than that of PS700. However, such a protection role was also dependent on BC concentration, the higher of which, the stronger the protective effect. For examples, the eDNA segments in BC systems with a solid/water ratio of 1:100 (Fig. 4b and c, lanes 6 and 7) were much larger than that with a solid/water ratio of 1:200 (Fig. 4b and c, lanes 2 and 3). In order to further understand the protection effect of BCs, we compared BCs with kaolinite since kaolinite could protect eDNA from DNase I effectively (Cai et al., 2006a). As shown in Fig. 4a, in the system of kaolinite with a solid/water ratio of 1:100, the electrophoresis pattern of eDNA with 1.6 μg/mL DNase I (lane 7) is almost the same as that of pristine eDNA (lane 14), indicating the eDNA was not degraded due to the protection from kaolinite, whereas the eDNA was degraded into much smaller segments in the presence of WC700 and PS700 at the same condition as kaolinite. This indicated that the protection effect of WC700 and PS700 was much lower than that of kaolinite. WS700 could not provide any protection for eDNA because eDNA was completely degraded by DNase I even at a concentration 0.8 μg/mL (Fig. 4d).

Among the three types of BCs, WC700 having the lowest adsorption of eDNA had the highest capability of protecting eDNA against degradation by DNase I. This suggests that the degradation of eDNA in BC system could not be governed by the adsorption of eDNA on BCs. Previous studies proposed that the configuration change of eDNA on adsorbents might be responsible for the protection of eDNA against enzymatic degradation, because it may prevent nuclease from recognizing or interacting with appropriate binding sites on the eDNA (Stotzky, 2000). However, Cai et al. (2006a) found that changes in eDNA structure after binding on soil colloids and minerals had a minor influence on its resistance to enzymatic degradation. In the present study, the resistance to nuclease degradation was independent of eDNA configuration, because it did not change after the adsorption on BCs. In order to identify whether the BC-bound eDNA can be degraded by nuclease or not, the degradation of BC-bound eDNA by free DNase I was conducted (scenarios 2). As shown in Fig. 5a, the absorbance at 260 nm of supernatant after the degradation by free DNase I was significantly higher than that of the control (background solution), but lower than that of the free eDNA at the same concentration. This means the concentration of eDNA segments in the supernatant of degradation system with BC-bound eDNA was lower than that in the absence of BCs; the BC-bound eDNA was partly degraded by DNase I. It is possible that the BC adsorption lowered the availability of eDNA to DNase I. The result of electrophoresis showed that the size of degraded eDNA fragments was smaller than 100 bp, as indicated by the absence of eDNA bands on electrophoresis tap (Fig. 5b). Furthermore, the absorbance of degradation supernatant (the supernatant of mixture of BC-bound eDNA and DNase I) decreased in the order of WS700 > PS700 > WC700 (Fig. 5a), suggesting the WC700 bound eDNA was degraded the least by DNase I. Consequently, it confirmed that WC700 provided the strongest protection for eDNA against enzymatic degradation among the three tested BCs.

Adsorption of nucleases on solid particles could result in inactivation of enzyme activity and a reduction in biodegradation (Cai et al., 2006a; Khanna and Stotzky, 1992). The degradation of free eDNA by BC-bound DNase I was also conducted (scenario 3). As shown in Fig. 5b (lane 2–7), the eDNA bands in the system of BCs-bound DNase I are almost the same as that of the free eDNA, indicating that the BCs-bound nuclease had almost lost its degradability to eDNA. Consequently, in the coexistence system of BC, eDNA, and DNase I, the adsorption of DNase I by BC would directly affect the degradability of DNase I to eDNA, the higher the adsorption on DNase I, the higher the inhibition of degradation. The adsorption results of DNase I on BCs supported this hypothesis (Appendix A Fig. S5). The adsorption of DNase I on BCs decreased in the order WC700 > PS700 > WS700, consistent with the order of their capabilities of protecting eDNA against degradation. These re-

sults confirmed that the protection of eDNA by BCs against enzymatic degradation was related to the adsorption of the nuclease.

3. Conclusions

The current research advances our understanding of the interaction between eDNA and aromatized BCs. The eDNA was irreversibly adsorbed by aromatized BC. Electrostatic interaction, Ca ion bridge interactions, and π-π interactions between eDNA and BCs could dominate the adsorption, while ligand exchange and hydrophobic interactions were not the main driving force. Aromatized BCs could protect eDNA from DNase I degradation to a certain extent, which was governed by the adsorption of nuclease on BCs rather than by the adsorption of eDNA on BCs. BC-bound eDNA could be partly degraded by nuclease, while BC-bound nuclease completely lost its degradability. These results highlight that the fate of eDNA in soil and aquatic environments can be significantly affected by BC. In the future, the effect of BC colloids on the mobility eDNA need to be further explored because the strong and irreversible adsorption of eDNA on BC provides the possibility for the co-transport of eDNA with BC colloids in the environment.

Acknowledgments

This work was supported by the National Natural Science Foundation of China (Nos. 21976158, 21525728, and 21677129).

Appendix A Supplementary data

Supplementary material associated with this article can be found, in the online version, at doi:10.1016/j.jes.2020.08.017.

REFERENCES

Adamson, A.W., 1990. Physical Chemistry of Surfaces, 5th ed. John Wiley & Sons, Inc., New York.

Ahmad, M., Rajapaksha, A.U., Lim, J.E., Zhang, M., Bolan, N., Mohan, D., et al., 2014. Biochar as a sorbent for contaminant management in soil and water: a review. Chemosphere 99, 19–33.

Ahmed, T., Kilina, S., Das, T., Haraldsen, J.T., Rehr, J.J., Balatsky, A.V., 2012. Electronic fingerprints of DNA bases on graphene. Nano Lett. 12, 927–931.

Allen, S.J., Mckay, G., Porter, J.F., 2004. Adsorption isotherm models for basic dye adsorption by peat in single and binary component systems. J. Colloid Interface Sci. 280, 322–333.

Azizian, S., 2004. Kinetic models of sorption: a theoretical analysis. J. Colloid Interface Sci. 276, 47–52.

Banyay, M., Gräslund, A., 2002. Structural effects of cytosine methylation on DNA sugar pucker studied by FTIR. J. Mol. Biol. 324, 667–676.

Cáceres-Jensen, L., Rodriguez-Becerra, J., Parra-Rivero, J., Escudey, M., Barrientos, L., Castro-Castillo, V., 2013. Sorption kinetics of diuron on volcanic ash derived soils. J. Hazard. Mater. 261, 602–613.

Cai, P., Huang, Q.Y., Chen, W., Zhang, D., Wang, K.Z., Jiang, D., et al., 2007. Soil colloids-bound plasmid DNA: Effect on transformation of E. coli and resistance to DNase I degradation. Soil Biol. Biochem. 39, 1007–1013.

Cai, P., Huang, Q.Y., Li, M., Liang, W., 2008. Binding and degradation of DNA on montmorillonite coated by hydroxyl aluminum species. Colloid Surf. B 62, 299–306.

Cai, P., Huang, Q.Y., Zhang, X.W., 2006a. Interactions of DNA with clay minerals and soil colloidal particles and protection against degradation by DNase. Environ. Sci. Technol. 40, 2971–2976.

Cai, P., Huang, Q.Y., Zhang, X.W., Chen, H., 2006b. Adsorption of DNA on clay minerals and various colloidal particles from an Alfisol. Soil Biol. Biochem. 38, 471–476.

Chen, B., Zhou, D., Zhu, L., 2008. Transitional adsorption and partition of nonpolar and polar aromatic contaminants by biochars of pine needles with different pyrolytic temperatures. Environ. Sci. Technol. 42, 5137–5143.

Chen, Z., Chen, B., Chiou, C.T., 2012. Fast and slow rates of naphthalene sorption to biochars produced at different temperatures. Environ. Sci. Technol. 46, 11104–11111.

Dai, Z.M., Webste, T.M., Enders, A., Hanley, K.L., Xu, J.M., Thies, J.E., et al., 2017. DNA extraction efficiency from soil as affected by pyrolysis temperature and extractable organic carbon of high-ash biochar. Soil Biol. Biochem. 115, 129–136.

Demaneche, S., Monrozier, L.J., Quiquampoix, H., Simonet, P., 2001. Evaluation of biological and physical protection against nuclease degradation of clay-bound plasmid DNA. Appl. Environ. Microb. 67, 293–299.

Fang, J., Shan, X.Q., Wen, B., Lin, J.M., Lu, X.C., Liu, X.D., et al., 2008. Sorption and desorption of phenanthrene onto iron, copper and silicon dioxide nanoparticles. Langmuir 24, 10929–10935.

Hale, L., Crowley, D., 2015. DNA extraction methodology for biochar-amended sand and clay. Biol. Fert. Soils 51, 733–738.

Hammes, K., Smernik, R.J., Skjemstad, J.O., Herzog, A., Vogt, U.F., Schmidt, M.W.I., 2006. Synthesis and characterisation of laboratory-charred grass straw (Oryza sativa) and chestnut wood (Castanea sativa) as reference materials for black carbon quantification. Org. Geochem. 37, 1629–1633.

Han, L.F., Ro, K.S., Wang, Y., Sun, K., Sun, H.R., Librad, J.A., et al., 2018. Oxidation resistance of biochars as a function of feedstock and pyrolysis condition. Sci. Total. Environ. 616-617, 335–344.

Heller, D.A., Jeng, E.S., Yeung, T.K., Martinez, B.M., Moll, A.E., Gastala, J.B., et al., 2006. Optical detection of DNA conformational polymorphism on single-walled carbon nanotubes. Science 311, 508–511.

Hou, Y.K., Wu, P.X., Huang, Z.J., Ruan, B., Liu, P.Y., Zhu, N.W., 2014. Successful intercalation of DNA into CTAB-modified clay minerals for gene protection. J. Mater. Sci. 49, 7273–7281.

Jin, H., 2010. Characterization of Microbial Life Colonizing Biochar and Biochar Amended Soils. Cornell University, Ithaca, NY Ph.D..

Keiluweit, M., Nico, P.S., Johnson, M.G., Kleber, M., 2010. Dynamic molecular structure of plant biomass-derived black carbon (biochar). Environ. Sci. Technol. 44, 1247–1253.

Khanna, M., Stotzky, G., 1992. Transformation of Bacillus subtilis by DNA bound on montmorillonite and effect of DNase on the transforming ability of bound DNA. Appl. Environ. Microb. 58, 1930–1939.

Kypr, J., Kejnovská, I., Renčiuk, D., Vorlíčková, M., 2009. Circular dichroism and conformational polymorphism of DNA. Nucleic Acids Res. 37, 1713–1725.

Li, F.Y., Cao, X.D., Zhao, L., Wang, J.F., Ding, Z.L, 2014. Effects of mineral additives on biochar formation: carbon retention, stability, and properties. Environ. Sci. Technol. 48, 11211–11217.

Lian, F., Xing, B.S., 2017. Black carbon (biochar) in water/soil environments: molecular structure, sorption, stability, and potential risk. Environ. Sci. Technol. 51, 13517–13532.
Lin, D.H., Pan, B., Zhu, L.Z., Xing, B.S., 2007. Characterization and phenanthrene sorption of tea leaf powders. J. Agric. Food Chem. 55, 5718–5724.
Ma, J.F., Takahashi, E., 2002. Soil, fertilizer, and plant silicon research in Japan. In: Chapter 5: Silicon-accumulating Plants in the Plant Kingdom. Elsevier B.V., pp. 63–67. doi:10.1016/B978-044451166-9/50005-1.
Mady, M.M., Mohammed, W.A., El-Guendy, N.M., Elsayed, A.A., 2011. Interaction of DNA and polyethylenimine: Fourier transform infrared (FTIR) and differential scanning calorimetry (DSC) studies. Int. J. Phys. Sci. 6, 7328–7334.
Mao, D., Luo, Y., Mathieu, J., Wan, Q., Feng, L., Mu, Q., et al., 2014. Persistence of extracellular DNA in river sediment facilitates antibiotic resistance gene propagation. Environ. Sci. Technol. 48, 71–78.
Nguyen, B.T., Lehmann, J., 2009. Black carbon decomposition under varying water regimes. 2009. Org. Geochem. 40, 846–853.
Nguyen, T.H., Chen, K.L., 2007. Role of divalent cations in plasmid DNA adsorption to natural organic matter-coated silica surface. Environ. Sci. Technol. 41, 5370–5375.
Ochman, H., Lawrence, J.G., Grosiman, E.A., 2000. Lateral gene drugs and a double-stranded oligonucleotide studied by electransfer and the nature of bacterial innovation. Nature 405, 299–304.
Oliveira, R., Amaro, F., Azevedo, M., Vale, N., Gonçalves, H., Antunes, C., et al., 2019. New voltammetric and spectroscopic studies to quinacrine-DNA-Cdots interaction. Electrochim. Acta 306, 122–131.
Önal, Y., 2006. Kinetics of adsorption of dyes from aqueous solution using activated carbon prepared from waste apricot. J. Hazard. Mater. 137, 1719–1728.
Peng, B., Chen, L., Que, C., Yang, K., Deng, F., Deng, X., et al., 2016. Adsorption of antibiotics on graphene and biochar in aqueous solutions induced by π-π interactions. Sci. Rep. 6, 31920–31929. doi:10.1038/srep31920.
Pietramellara, G., Ascher, J., Borgogni, F., Ceccherini, M.T., Guerri, G., Nannipieri, P., 2009. Extra cellular DNA in soil and sediment: fate and ecological relevance. Biol. Fert. Soils 45, 219–235.
Porkodi, K., Vasanth Kumar, K., 2007. Equilibrium, kinetics and mechanism modeling and simulation of basic and acid dyes sorption onto jute fiber carbon: eosin yellow, malachite green and crystal violet single component systems. J. Hazard. Mater. 143, 311–327.
Qian, L., Zhang, W., Yan, J., Han, L., Gao, W., Liu, R., et al., 2016. Effective removal of heavy metal by biochar colloids under different pyrolysis temperatures. Bioresour. Technol. 206, 217–224.
Rajapaksha, A.U., Vithanage, M., Zhang, M., Ahmad, M., Mohan, D., Chang, S.X., et al., 2014. Pyrolysis condition affected sulfamethazine sorption by tea waste biochars. Bioresour. Technol. 166, 303–308.
Rojas, F., Kornhauser, I., Felipe, C., Cordero, S., 2001. Everett's sorption hysteresis domain theory revisited from the point of view of the dual site-bond model of disordered media. J. Mol. Catal. – Chem. 167, 141–155.
Roxbury, D., Manohar, S., Jagota, A., 2010. Molecular simulation of DNA B-sheet and B-barrel structures on graphite and carbon nanotubes. J. Phys. Chem. C 114, 13267–13276.
Saeki, K., Ihyo, Y., Sakai, M., Kunito, T., 2011. Strong adsorption of DNA molecules on humic acids.. Environ. Chem. Lett. 9, 505–509.
Saeki, K., Sakai, M., Wada, S.I., 2010b. DNA adsorption on synthetic and natural allophones. Appl. Clay Sci. 50, 493–497.
Sander, M., Lu, Y.F., Pignatello, J.J., 2005. A thermodynamically based method to quantify true sorption hysteresis. J. Environ. Qual. 34, 1063–1072.
Sheng, X., Qin, C., Yang, B., Hua, X.J., Liu, C., Waigia, M.G., et al., 2019. Metal cation saturation on montmorillonites facilitates the adsorption of DNA via cation bridging. Chemosphere 235, 670–678.
Song, B., Chen, M., Zhao, L., Qiu, H., Cao, X., 2019. Physicochemical property and colloidal stability of micron- and nano-particle biochar derived from a variety of feedstock sources. Sci. Total Environ. 661, 685–695.
Stotzky, G., 2000. Persistence and biological activity in soil of insecticidal proteins from Bacillus thuringiensis and of bacterial DNA bound on clays and humic acids. J. Environ. Qual. 29, 691–705.
Sun, J.X., Li, Y., Lin, J.P., 2017. Studying the adsorption of DNA nanostructures on graphene in the aqueous phase using molecular dynamic simulations. J. Mol. Graph. Model. 74, 16–23.
Sun, X.G., Cao, E.H., Zhang, X.Y., Liu, D.G., Bai, C.L., 2002. The divalent cation-induced DNA condensation studied by atomic force microscopy and spectral analysis. Inorg. Chem. Commun. 5, 181–186.
Tran, H.N., Wang, Y.F., You, S.J, Chao, H.P., 2017. Insights into the mechanism of cationic dye adsorption on activated charcoal: the importance of π-π interactions. Process. Saf. Environ. 107, 168–180.
Uchimiya, M., Wartelle, L.H., Lima, I.M., Klasson, K.T., 2010. Sorption of deisopropylatrazine on Broiler litter biochars. J. Agric. Food Chem. 58, 12350–12356.
Wang, C.Y., Wang, T., Li, W.B., Yan, J.F., Li, Z.B., Ahmad, R., et al., 2014. Adsorption of deoxyribonucleic acid (DNA) by willow wood biochars produced at different pyrolysis temperatures. Biol. Fert. Soils 50, 87–94.
Wang, D., Zhang, W., Hao, X., Zhou, D., 2013. Transport of biochar particles in saturated granular media: effects of pyrolysis temperature and particle size. Environ. Sci. Technol. 47 (2), 821–828.
WHO, 2015. Global Action Plan on Antimicrobial Resistance.
Wu, W.H., Jiang, W., Zhang, W.D., Lin, D.H., Yang, K., 2013. Influence of functional groups on desorption of organic compounds from carbon nanotubes into water: insight into desorption hysteresis. Environ. Sci. Technol. 47, 8373–8382.
Xiao, X., Chen, B., Zhu, L., 2014. Transformation, morphology, and dissolution of silicon and carbon in rice straw-derived biochars under different pyrolytic temperatures. Environ. Sci. Technol. 48, 3411–3419.
Yang, H., Zheng, K., Zhang, Z.M., Shi, W., Jing, S.B., Wang, L., et al., 2012. Adsorption and protection of plasmid DNA on mesoporous silica nanoparticles modified with various amounts of organosilane. J. Colloid Interface Sci. 369, 317–322.
Yang, K., Jiang, Y., Yang, J.J., Lin, D.H., 2018. Correlations and adsorption mechanisms of aromatic compounds on biochars produced from various biomass at 700°C. Environ. Pollut. 233, 64–70.
Zeng, S., Chen, L., Wang, Y., Chen, J., 2015. Exploration on the mechanism of DNA adsorption on graphene and graphene oxide via molecular simulations. J. Phys. D: Appl. Phys. 48, 275402. doi:10.1088/0022-3727/48/27/275402.
Zhang, Y., Li, A., Dai, T., Li, F., Xie, H., Chen, L., et al., 2018a. Cell-free DNA: a neglected source for antibiotic resistance genes spreading from WWTPs. Environ. Sci. Technol. 52, 248–257.
Zhang, K., Chen, B., Mao, J., Zhu, L., Xing, B., 2018b. Water clusters contributed to molecular interactions of ionizable organic pollutants with aromatized biochar via p-PAHB: sorption experiments and DFT calculations. Environ. Pollut. 240, 342–352.

Zhao, X., 2011. Self-assembly of DNA segments on graphene and carbon nanotube arrays in aqueous solution: a molecular simulation study. J. Phys. Chem. C 115, 6181–6189.
Zheng, H., Wang, Z., Zhao, J., Herbert, S., Xing, B.S., 2013. Sorption of antibiotic sulfamethoxazole varies with biochars produced at different temperatures. Environ. Pollut. 181, 60–67.
Zhou, Y.L., Li, Y.Z., 2004. Studies of interaction between poly (allylamine hydrochloride) and double helix DNA by spectral methods. Biophys. Chem. 107, 273–281.